

## Beam Position Monitoring System at CESR

---

**M.G.Billing, W.F.Bergan, M.J.Forster, R.E.Meller, M.C.Rendina, N.T.Rider, D.C.Sagan, J.Shanks, J.P.Sikora, M.G.Stedinger, C.R.Strohman, Cornell Laboratory for Accelerator-based ScienceS and Education (CLASSE), Cornell University, 161 Synchrotron Dr., Ithaca, NY, 14850, U.S.A.**

**M.A.Palmer, Collider Accelerator Department, Brookhaven National Laboratory, P.O.Box 5000, Upton, NY, 11973-5000, U.S.A.**

**R.L.Holtzapple, California Polytechnic State University, Physics Department, 1 Grand Ave, San Luis Obispo, CA, 93407, U.S.A.**

**ABSTRACT:** The Cornell Electron-positron Storage Ring (CESR) has been converted from a High Energy Physics electron-positron collider to operate as a dedicated synchrotron light source for the Cornell High Energy Synchrotron Source (CHESS) and to conduct accelerator physics research as a test accelerator, capable of studying topics relevant to future damping rings, colliders and light sources. Some of the specific topics that were targeted for the initial phase of operation of the storage ring in this mode, labeled CESRTA (CESR as a Test Accelerator), included 1) tuning techniques to produce low emittance beams, 2) the study of electron cloud development in a storage ring and 3) intra-beam scattering effects. The complete conversion of CESR to CESRTA occurred over a several year period and is described elsewhere[1], [2], [3]. As a part of this conversion the CESR beam position monitoring (CBPM) system was completely upgraded to provide the needed instrumental capabilities for these studies. This paper describes the new CBPM system hardware, its function and representative measurements performed by the upgraded system.

**KEYWORDS:** Accelerator Subsystems and Technologies, Beam-line Instrumentation

---

## Contents

<b>1</b>	<b>BPM Design</b>	<b>1</b>
1.1	System Requirements	1
1.2	System Design	2
<b>2</b>	<b>Measurements and Characterization</b>	<b>5</b>
2.1	Acquisition of Position and Trajectory Data	5
2.2	Estimating Position Uncertainties	6
2.3	Measurements of Betatron Phase Advance and Coupling	10
2.4	Status and Performance	11
<b>3</b>	<b>Summary</b>	<b>13</b>

---

## 1 Instrument Requirements and Design

The CESR-TA project[1–3] required the development or upgrading of several systems involved in accelerator operations. In particular, a significant upgrade was needed for the beam position monitor (BPM) system, which replaced an original relay-based position monitor system. The new individual readout modules for each BPM are capable of turn-by-turn and bunch-by-bunch trajectory measurements for bunches spaced as closely as 4 nsec or counter-rotating bunches with a 14 nsec spacing.

The upgraded readout for the BPM system that provides high resolution measurement capability has been designed and deployed. This system provides turn-by-turn measurements of individual bunches within bunch trains with spacings that are multiples of either 4 nsec or 14 nsec. The system has the ability to measure betatron phase, and coupling via synchronous detection of a driven beam. This paper is the concluding document in a sequence preliminary and supplementary papers and reports on the CBPM system in publications[4–6] at accelerator conferences[7–12] and within the report on progress for the CESR-TA Project in the CESR-TA Phase 1 Report[13]. Substantial sections of the paper for the accelerator conference proceedings for IPAC 10[11] have been reproduced here verbatim.

### 1.1 System Requirements

The primary operational requirements for the CBPM system include:

- The ability to operate with counter-rotating beams of electrons and positrons in a single vacuum chamber for two-beam synchrotron light operations for CHESS;
- High resolution for low emittance optics correction and tuning;
- Turn-by-turn readout capability for multiple bunches to support beam dynamics studies;

- Capability for digitizing single species bunch trains with bunch spacing as small as 4 nsec and dual beam digitization for bunch trains with 14 nsec spacing.

The need for dual beam operation of the system places a unique constraint on the CESR BPM specifications. Since the relative arrival time of the bunches from the two beams varies widely from location to location around the ring, standard RF processing techniques to optimize resolution and minimize timing sensitivity cannot be applied to the full system. As a result, the CESR design utilizes peak sampling with a high bandwidth digitizer and incorporates hardware and software design features to optimize the system timing performance. Table 1 summarizes the design specifications for the high resolution measurements required for low emittance optics correction [11].

**Table 1.** CESR BPM Module Requirements[11].

Parameter	Specification
Front End Bandwidth (required for 4 ns bunch trains)	500 MHz
Absolute Position Accuracy (long term)	100 $\mu\text{m}$
Single Shot Position Resolution	10 $\mu\text{m}$
Differential Position Accuracy	10 $\mu\text{m}$
Channel-To-Channel Sampling Time Resolution	10 psec

## 1.2 System Design

The CESR BPM system consists of a network of local sensors and processors. Each location has four beam buttons arranged in a mirror symmetric fashion, an example of which is shown in Figure 1, providing signals for each processing module. The relative amplitude of the four BPM electrodes yields horizontal and vertical position and beam intensity information. All modules share a common control database, timing and synchronization controls, and networked data storage. This allows for accelerator-wide coordinated measurements.

Figure 2 shows a block diagram of the digital BPM readout modules developed for CESR. Each module incorporates four front end boards each with two parallel 16-bit digitizer chains based on the Analog Devices AD9461 operating with digitization rates up to 125 MHz. When operating with 4 ns bunch trains, digitizing is interleaved between the two chains. For 14 ns dual species operation, each digitizer chain handles a single species. The front end boards have 1) a fixed gain amplifier optimized for precision measurements for bunches with  $N_b \sim 1 \times 10^{10}$  particles and 2) a digitally-controlled variable gain amplifier permitting measurements over a wide dynamic range for the beam current.

The timing configuration is implemented by a dedicated timing board integral within each module, which takes as an input a three-temporal-state 24 MHz clock reference signal from the CESR master timing system. As seen in Figure 3 the rising clock edges are phase-locked to a 24 MHz clock on the timing board. The second timing slot per 24 MHz period encodes 1) a turns marker signal, a signal selecting the turn for all CBPM modules to initiate data acquisition, 2) two hardware triggers (to initiate synchronous data acquisition), 3) 8 bits for a software command word, and 4) the 9-bit phases for each of the two phase lock loops from the (horizontal, and vertical) tune

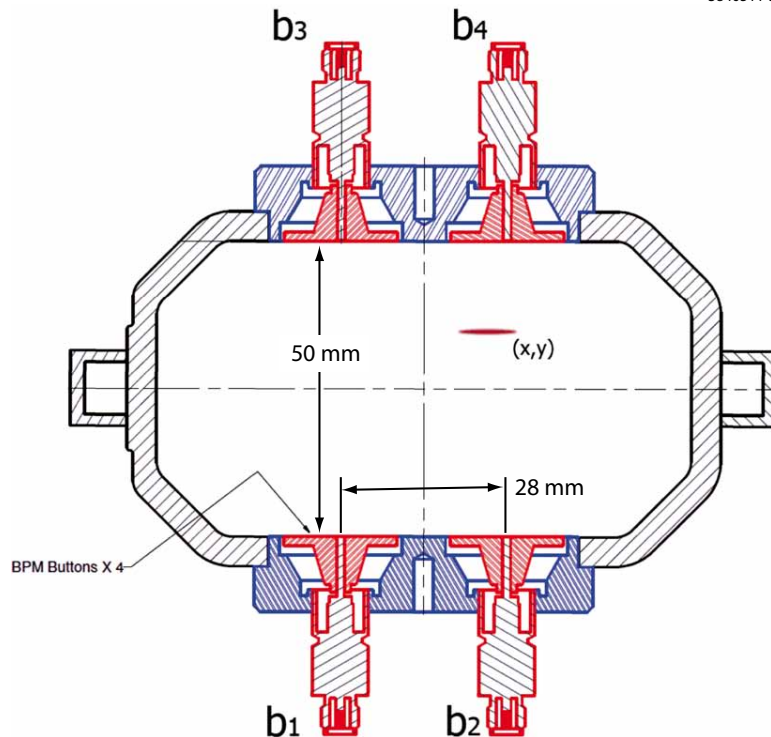


**Figure 1.** BPM detector as configured in one of the superconducting wiggler vacuum chambers.

trackers. To avoid a timing slew as the bit pattern changes, the data is encoded into every other 24 MHz period and its complement is encoded into the immediately following 24 MHz period. The turns marker signal is not encoded as ordinary data, instead it is encoded as a "code violation". For the turns marker, the sequencing of bit and complement of that bit is violated by sending the same state in 3 consecutive bits. This could never happen with ordinary data. There is also a guard bit that follows normal complementing at each end of this 3-bit stream, hence the use of 5 of the 61 bits to encode the turns marker. The timing board provides overall digitization rate control, adjustment capability for channel-to-channel digitization time delays, and global adjustment capability for the module digitization time relative to the bunch arrival time at the detector. The timing delays have a resolution of  $\Delta t_{\text{step}} = 10$  psec and this degree of local timing adjustment is required to sample at the peak of each BPM signal in order to maintain the resolution and noise performance for each device.

Communications, operational control, and onboard data processing for each device is provided through a digital board and TigerSharc digital signal processor (DSP). Communication is supported for both ethernet and the dedicated CESR field bus, Xbus[14, 15].

The CESR BPM system is controlled via custom server applications running on the CESR control system cluster. All system parameters, including pedestal and gain scale calibration values, delay tables for all supported bunch spacing configurations, and various identification and management data, are stored in a central location. Each server application is responsible for loading, managing, and saving this information with new values generated within the instruments. All control and data read back is performed via a custom network protocol[16] running over 100 Mbit

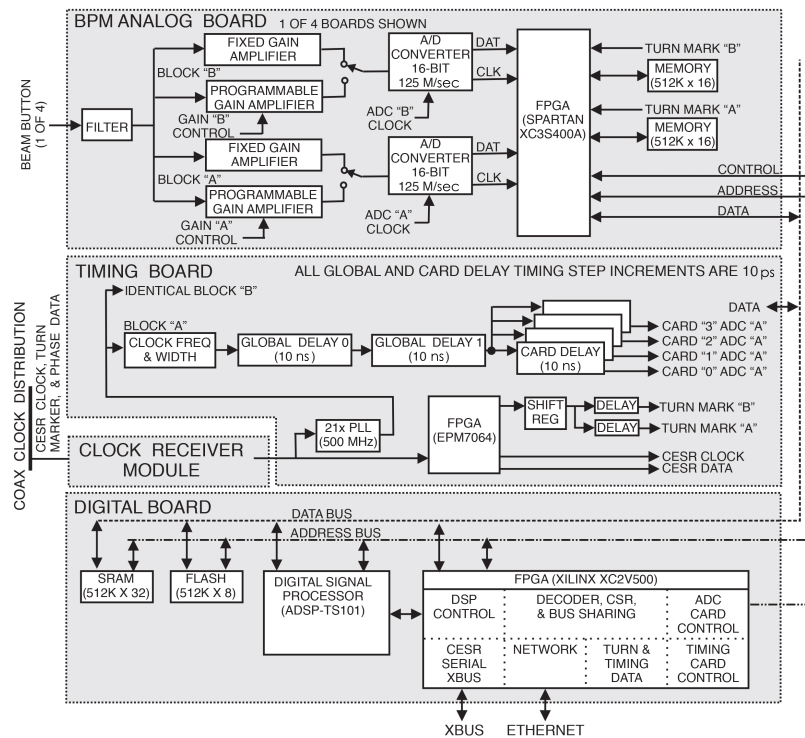


Figure 2. BPM module functional diagram[11].

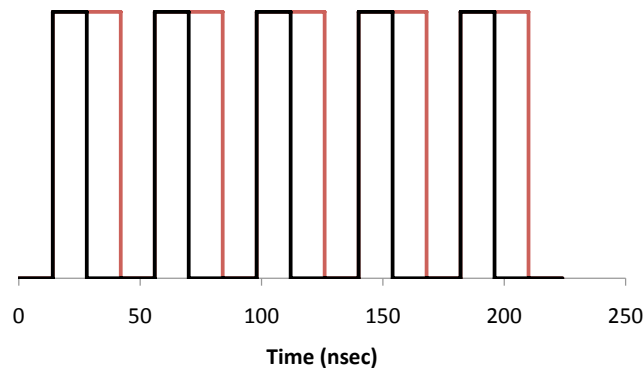


Figure 3. Example of a CBPM 24 MHz timing signal. The black portion of the waveform is the same for all periods of the timing signal. The red portion of the waveform may be a digital high or low in order to carry a single bit of information for that clock period. In the next clock period the digital sense of the red signal is reversed in order to prevent a DC shift in the waveform, which would depend on the information being carried in that third timing state. (A DC shift of the waveform could add jitter to the timing edges.) As there are 61 periods of the 24 MHz signal per CESR turn, the trigger signal actually encodes 28 bits of information, which is sent to all modules per turn.

ethernet.

Rapid measurements, taking advantage of on-board averaging, pedestal subtraction, and gain scaling can be requested of all or a subset of instruments or detailed turn-by-turn data can be

acquired for an arbitrary combination of bunches and turns in 14 ns or 4 ns bunch spacing modes. The software on board the instruments is also capable of automatically determining appropriate delays to use for sampling at the optimal point of the incoming waveform on all channels.

Data from all detectors are stored in a centrally-located database. Raw ADC values, along with pedestals and gain scale factors for all channels and amplifier settings are stored in all data files. Sufficient information is provided to allow analysis of raw ADC or pedestal-subtracted and gain-scaled turn-by-turn button data and/or physical beam positions for every bunch stored and detector location in the machine.

## 2 Measurements and Characterization

### 2.1 Acquisition of Position and Trajectory Data

Position data may be acquired in two basic modes: orbit data and turn-by-turn trajectory data. For turn-by-turn measurements the acquisition in all CBPM modules is initiated by a trigger bit appearing in the timing signal. This bit is typically timed to occur several CESR periods ( $2.56 \mu\text{sec}$ ) before the turn during which beam transfer would occur from the Synchrotron injector into CESR. This permits the measuring of injected beam into CESR, when there is no stored beam. Since the transfer trigger is synchronous with the 60 Hz mains frequency  $\pm 75 \mu\text{sec}$  (the delay to align the timing of bunches in the Synchrotron injector and CESR) and the number of turns may be chosen to span an integer number of mains frequency cycles, any averaging over such a span would produce the same average when performed for different measurements.

The incoming signals are filtered to produce a waveform with a longer time shape to reduce the sensitivity to the sampling time. Since the signal coming from the button electrode is essentially a differentiated gaussian, after filtering, the signal shape for a positron bunch becomes a 500 MHz sine-wave. The initial end of the 500 MHz signal connects smoothly to the DC baseline with an approximately constant curvature arc. Figure 4 shows a sampling time scan for the four electrode signals at one CBPM modules. After filtering, the sinusoidal portion of the waveform shape for the button signal from the n-th electrode,  $b_n(t)$ , may be written as a function of time in terms of the peak signal  $\hat{b}_n$  as

$$b_n(t) = \hat{b}_n \cos\{2\pi f(t + \Delta t_n)\} \quad (2.1)$$

where n ranges from 1 to 4,  $\Delta t_n$  is the average temporal offset of the sampling gate with respect to the first peak of the waveform and  $f$  is approximately 500 MHz.

During orbit measurements typically the four electrode signals are acquired for 1024 turns. For small displacements each electrode's signal is averaged and the average x- and y-positions are computed using

$$\begin{aligned} x &= k_x \frac{\Delta_x}{\Sigma} \\ y &= k_y \frac{\Delta_y}{\Sigma} \end{aligned} \quad (2.2)$$

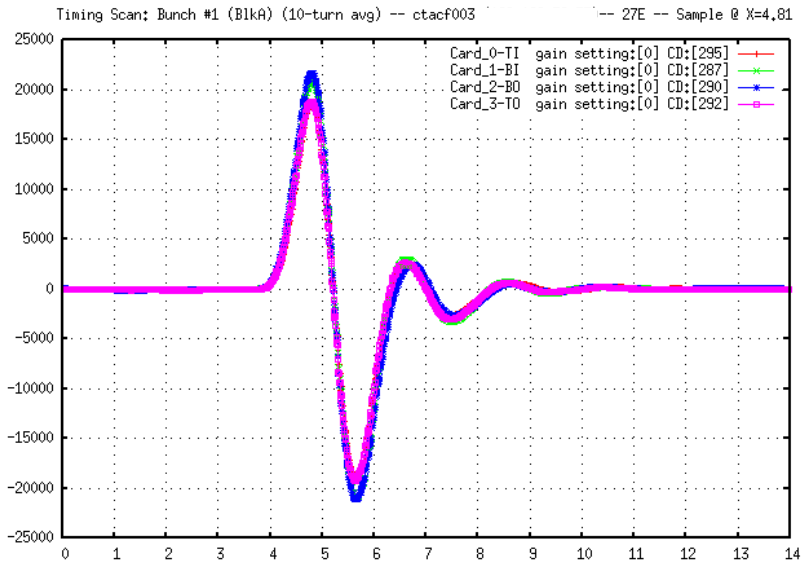


**Figure 4.** Timing scan of the four BPM electrodes from BPM27E with the beam nearly on-axis using the fixed gain channel with a positron bunch of 0.75 mA. The vertical scale is digitizer units and the horizontal scale is nsec. Each point of the scan is a ten turn average. The difference in the effective period of the oscillation present in these filtered signals is due to the tolerances of the filter components.

where  $\Delta_x$  is the difference of the radial outside electrodes minus the radial inside electrodes,  $\Delta_y$  is the difference of the upper electrodes minus the lower electrodes and  $\Sigma$  is the sum of all four electrodes. The vacuum chamber-specific geometry factors,  $k_x$  and  $k_y$ , are given in Table 2 for the different types of vacuum chambers in CESR.

**Table 2.** Geometric Factors for Different CESR Vacuum Chamber Cross Sections

Vacuum Chamber Geometry	$k_x$ (mm)	$k_y$ (mm)
Normal CESR Cross Section (50 mm x 90 mm)[4]	26.2	19.6
CESR Round Cross Section (45.0 mm inner radius)[17]	22.5	22.5
Undulator Cross Section (5 mm x 70 mm)[18]	2.43	1.83

For turn-by-turn trajectories the number of turns may be chosen in the calling sequence to the CBPM servers. One of the trigger bits within the timing signal starts the turn-by-turn digitization of the electrode signals. After acquiring the complete set of data, the positions are computed turn by turn using the same formulae as the orbit data. The entire position sequence is returned and stored in a raw data file.

## 2.2 Estimating Position Uncertainties

The uncertainties in position measurements  $\delta x, \delta y$  may be directly attributed to the uncertainty in individual button signals  $\delta b_n/b_n$ . Starting from Eqn. 2.2:

$$\delta x = \sqrt{\sum_n \left( \frac{\partial x}{\partial b_n} \delta b_n \right)^2}, \quad \text{where}$$

$$\left| \frac{\partial x}{\partial b_n} \right| = k_x \left| \frac{1}{\Sigma} \pm \frac{\Delta_x}{\Sigma^2} \right| \quad (2.3)$$

If the beam is well-centered in the vacuum chamber, all four button amplitudes  $b_n$  will be comparable, and their uncertainties  $\delta b_n$  will also be comparable. Thus,  $\Delta_x \approx 0$  and  $\left| \frac{\partial x}{\partial b_n} \right| \approx \left| \frac{k_x}{\Sigma} \right| \approx \frac{1}{4} \left| \frac{k_x}{b_n} \right|$ , and

$$\delta x \cong \sqrt{4 \left( \frac{\partial x}{\partial b_n} \delta b_n \right)^2}$$

$$\cong \frac{1}{2} k_x \left| \frac{\delta b_n}{\hat{b}_n} \right| \quad (2.4)$$

The error propagation for  $\delta y$  yields a similar result:

$$\delta y \cong \frac{1}{2} k_y \left| \frac{\delta b_n}{\hat{b}_n} \right| \quad (2.5)$$

For BPM systems, which integrate over multiple bunch passages, noise from the analog-to-digital converters (ADCs) dominates  $\delta b_n / \hat{b}_n$ . For the CBPM fixed-gain processing channel, the noise level observed in the 16-bit digitizer is two least significant bits (LSB). If the electrode signals are approximately 75% of full scale to allow for off-axis trajectories, this implies that the amplitude measurement error  $\delta \hat{b}_n$  due to digitizer fractional sampling error is

$$\frac{\delta \hat{b}_n}{\hat{b}_n} \simeq (0.75)^{-1} \times 2^{-14}$$

$$= 8.1 \times 10^{-5} \quad (2.6)$$

For peak-detection BPMs with bunch-by-bunch resolution such as the CBPM system, one must also account for timing errors. Therefore, the single-turn position measurement plus its error should be estimated by including not only an amplitude measurement error  $\delta \hat{b}_n$  due to ADC noise, but also the timing offset of the gate  $\Delta t_n$  and sampling trigger jitter error  $\delta t$ . Thus, the measurement  $b_n(t)$  plus its uncertainty  $\delta b_n(t)$  are:

$$b_n(t) + \delta b_n(t) = \left( \hat{b}_n + \delta \hat{b}_n \right) \cos \{ 2\pi f(t + \delta t + \Delta t_n) \} \quad (2.7)$$

If the timing jitter is small, i.e.,  $2\pi f \delta t \ll 1$ , then to second order in  $\delta t$  the amplitude measurement error may be approximated as:

$$\delta b_n(t) \cong -2\pi^2 f^2 \hat{b}_n \cos\{2\pi f \Delta t_n\} \delta t^2 - 2\pi f \hat{b}_n \sin\{2\pi f \Delta t_n\} \delta t + \delta \hat{b}_n \cos\{2\pi f \Delta t_n\} \quad (2.8)$$



From this expression, it is clear that if the average timing offset  $\Delta t_n$  were exactly zero, the amplitude error would be strictly second order in  $\delta t$ , with no linear component. Additionally, this expression implies that, if all four electrode signals had the same average timing offset  $\Delta t_n$ , the error due to timing jitter  $\delta t$  would cause all four signals to scale together in amplitude, and would therefore not significantly affect the position measurements. However, as long as the relative timing offsets between the four electrode signals are different, the signal amplitude uncertainties will have a first-order dependence on the timing jitter  $\delta t$ .

If, in addition to the timing jitter  $\delta t$  being small, the gate timing error is also small (i.e.,  $2\pi f \Delta t_n \ll 1$ ), this simplifies further to:

$$\delta b_n(t) \cong -4\pi^2 f^2 \hat{b}_n \Delta t_n \delta t + \delta \hat{b}_n \quad (2.9)$$

Note that Eqn. 2.9 explicitly shows a first order dependence on  $\delta t$ .

As stated previously, the minimum timing delay step for each channel is  $\Delta t_{\text{step}} = 10$  psec, corresponding to  $\Delta t_{\text{min}} = \pm 5$  psec precision. The time-in process is independent for the four button channels on a given module, therefore the typical timing offsets between different digitizing channels is taken to be  $\Delta t_n = \sqrt{2} \times \Delta t_{\text{min}} = 7$  psec.

The typical timing jitter  $\delta t$  can be directly measured using the CBPM modules themselves. To do this, the sampling point is shifted to near the zero-crossing of the 500 MHz filtered BPM electrode signal shown in Fig. 4. At the zero-crossing, the relative amplitude error scales proportionally with the timing jitter  $\delta t$ :

$$\begin{aligned} \delta b_{n, \text{timing}}(t) &\cong \frac{\partial b_n(t)}{\partial t} \delta t \\ &= -2\pi f \hat{b}_n \sin\{2\pi f(t + \Delta t_n)\} \delta t \\ &\cong -2\pi f \hat{b}_n \delta t \end{aligned} \quad (2.10)$$

where the waveform is taken to be zero at the location of the greatest slope (i.e., no DC offset).

Turn-by-turn data was acquired for six BPM processors in 15 sequential sets of measurements of 16,384 turns, timed in at the zero-crossing to maximize sensitivity to timing jitter. Using this technique, the average timing jitter has been determined to be  $\delta t = 10.5$  psec. It is interesting to note if this data is analyzed in 64-turn blocks (corresponding to roughly three synchrotron oscillation periods), the RMS is  $\delta t = 1.1$  psec, roughly corresponding to the expected  $1/\sqrt{N}$  for random noise.

These timing errors will produce an uncorrelated variation in the button signals. Following Eqn. 2.9, the contribution from the gate timing  $\Delta t_n$  and timing jitter  $\delta t$  to the fractional amplitude error signal is:

$$\begin{aligned} \left| \frac{\delta b_n}{\hat{b}_n} \right|_{\text{timing}} &\cong 4\pi^2 f^2 \Delta t_n \delta t \\ &= 4\pi^2 (500 \text{ MHz})^2 (7 \text{ psec})(10.5 \text{ psec}) \\ &= 7.25 \times 10^{-4} \end{aligned} \quad (2.11)$$

The contributions from digitizing noise (Eqn. 2.6) and from timing jitter (Eqn. 2.11) to the relative signal amplitude are assumed to be uncorrelated, hence their contributions add in quadrature. This gives a net fractional uncertainty of  $\delta b_n/\hat{b}_n = 7.29 \times 10^{-4}$  for each of the electrode signals.

As a cross-check one can also directly measure the peak signal variation. Turn-by-turn data was again acquired for six BPM processors in 15 sequential sets of measurements of 16,384 turns, timed in at the peak of the 500 MHz waveform. This yields an average observed fractional variation of the peak button signal of  $3.7 \times 10^{-3}$ . This is a considerably larger variation compared to the calculated fractional uncertainty of  $\delta b_n/\hat{b}_n = 7.29 \times 10^{-4}$ . It is important to note that the direct measurement of the peak signal variation also includes true beam motion, which cannot be deconvolved from timing or ADC contributions.

If the button signals are now averaged in 64-turn blocks, the averaged fractional amplitude RMS becomes  $8.7 \times 10^{-4}$ , roughly comparable to the computed  $\frac{\delta b_n}{\hat{b}_n}$ , implying the button variations on timescales  $> 64$  turns are due to real beam motion. The fractional button signal error calculated from the pair-wise BPM button differences for the 64-turns averages is observed to be  $5.5 \times 10^{-4}$ , smaller than the expected  $\sqrt{2} \times (8.7 \times 10^{-4}) = 1.2 \times 10^{-3}$  RMS, if the noise were completely random. This implies that the button signals themselves are varying systematically on a longer timescale  $> 64$  turns, attributed to variation in the timing jitter  $\delta t$  for the four button signals. If the gate delays  $\Delta t_n$  were accurately determined to place the sampling point at the peak of all button signals, but the timing jitter  $\delta t$  for all buttons were moving back and forth over the quadratic peak of the signals in a synchronous manner, the individual button signals would show a variation. However, this variation would cancel out when examining the pair-wise button differences. Since the beam position is calculated from button differences, this effect would not impact position measurements. Therefore, if the measured peak amplitude variation is due to correlated timing deviations between the button signals, much of the timing variation will have no influence on the accuracy of the position measurements.

Therefore, the estimated position uncertainties for the standard CESR vacuum chamber cross section are

$$\delta x = \frac{1}{2} k_x \frac{\delta b_n}{\hat{b}_n} = \frac{1}{2} (28 \text{ mm}) (7.3 \times 10^{-4}) = 10.2 \text{ } \mu\text{m} \quad (2.12)$$

$$\delta y = \frac{1}{2} k_y \frac{\delta b_n}{\hat{b}_n} = \frac{1}{2} (25 \text{ mm}) (7.3 \times 10^{-4}) = 9.1 \text{ } \mu\text{m} \quad (2.13)$$

These estimates predict reasonable success for achieving the design goals. They may also be over-estimates, since it is assumed that the beam centroid was not moving during the preceding measurements.

A special diagnostic triplet location has been used to study the resolution and stability of the system. The triplet consists of three sets of detectors mounted in close proximity on a single vacuum chamber. The vertical trajectory is fitted turn-by-turn and the residuals to the fits give the error for the position measurements with beam motion removed. Figure 5 shows a set of residuals for the position measurements with beam motion removed. Figure 5 shows a set of residuals for vertical orbit differences between pairs of triplet detectors. The uncertainties shown in the plots are the computed uncertainties for single position measurements for a CBPM module, based on these data. The histograms include 256K turns of data (0.67 sec duration) taken simultaneously with each

detector. The effective resolution corresponds to the standard deviation of each distribution, which is consistent with our goal for the system and comparable to the single shot position resolution, which was estimated above.

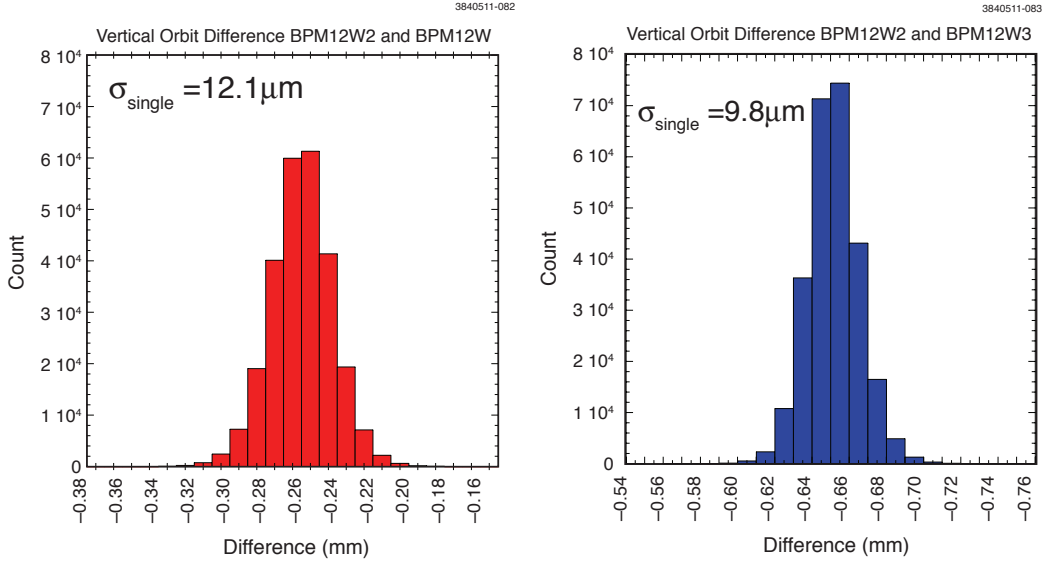


**Figure 5.** Vertical orbit residuals to the fitted trajectories between pairs of closely located detectors on a straight beam pipe at 12W (between quadrupoles 12W and 13W in CESR, the location of the CESR diagnostic triplet.) (The average differences not equaling zero indicate the absolute differences in the centers of the BPMs, which were not calibrated at the time of these measurements).

### 2.3 Measurements of Betatron Phase Advance and Coupling

The software processing in each CBPM module permits measurements of betatron phase and coupling. The basic formalism employed for extracting betatron phase advance from BPM data is described elsewhere[19]. Shaker magnets or stripline kickers, phased locked to a beam position sensor by devices called tune trackers, are utilized to resonantly excite a single bunch in CESR in the two normal dipole modes (corresponding to approximately horizontal and vertical). The phases of the tune tracker drives are digitized synchronously with each turn of the bunch circulating in CESR and these 9-bit digital values are inserted into the CBPM timing clock. When the CBPM modules are triggered to record turn-by-turn positions, they also record the tune tracker phase information turn-by-turn. After the data is acquired, the CBPM modules, utilizing lookup tables to reconstruct the trigonometric functions, integrate the position data to project the positions into the cosine-like and sine-like components with respect to the tune tracker's phase. This permits an accurate measurement of the beam's oscillation phase and amplitude even in the presence of variations in the betatron tunes. The cosine-like and sine-like components for each BPM electrode are returned to the CBPM servers for offline processing and analysis. Typically 40,960 turns of turn-by-turn data are acquired and analyzed for the betatron phase measurements to cover six periods of the 60 Hz mains frequency.

An example of a phase and coupling measurement relative to the optics design is shown in Figure 6. The phase measurements display betatron phase waves propagating at twice the betatron

phase advance. In the vertical, a quadrupole gradient error is clearly visible as a discontinuity for the average phase error near BPM detector 50. Figure 7 displays the preceding data after phase and coupling corrections have been applied.

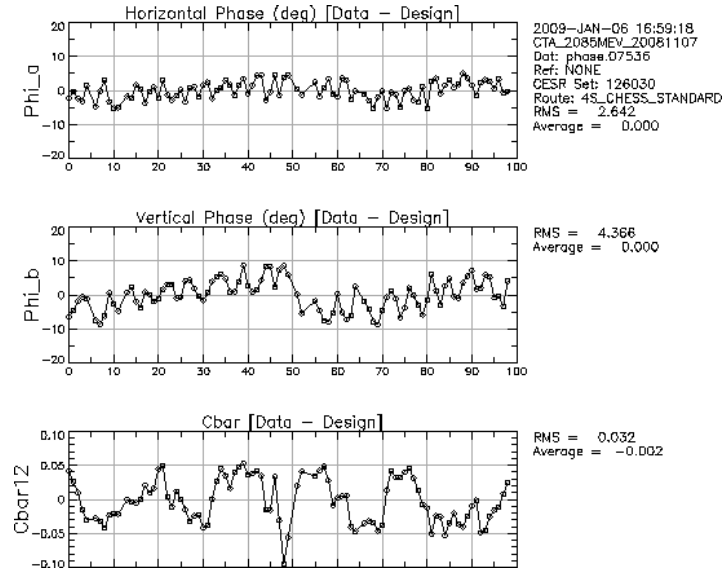


**Figure 6.** An example of a set of phase and coupling measurements. The two upper plots are the deviations from design for the betatron phases for the A-mode (horizontal-like) and B-mode (vertical-like) betatron dipole modes. The lower plot is the off-diagonal element of the  $\bar{C}$  horizontal-to-vertical coupling matrix. The horizontal scales on the plots are BPM number with the data set representing one complete cycle around CESR. The vertical scales for the phases are in degrees. The vertical scale for  $\bar{C}_{12}$  is unitless.

The uncertainty of the phase and coupling measurements has been estimated by recording a set of ten phase measurements in succession. The averages of the phase and  $\bar{C}_{12}$  coupling distributions has been computed detector by detector, resulting in the average RMS phase uncertainties for the horizontal phase of 0.060 degrees and for the vertical phase of 0.034 degrees and the average RMS  $\bar{C}_{12}$  uncertainty of  $6.9 \times 10^{-4}$ .

## 2.4 Status and Performance

Presently there are 110 digital BPM readout modules installed in CESR. Generally 100 of these modules are in routine use for beam diagnostics and machine studies with the remainder either available for orbit and trajectory measurements, for bunch-by-bunch current monitoring or for instrumentation hardware and software diagnostics. The BPM system has regularly been used to measure the bunch-by-bunch positions of a train of 4 ns spaced bunches with a minimum of cross talk between bunch signals.

The hardware and infrastructure of the CESR BPM system has been functioning since 2009 and has been in active use since its installation. Although the CBPM system is in routine use at CESR, development continues for improvements in data storage, analysis and diagnostic software.

Some of the development work that is in progress using CBPM module includes 1) the installation of 3 BPMs in each of the electron and positron transport lines from the Synchrotron

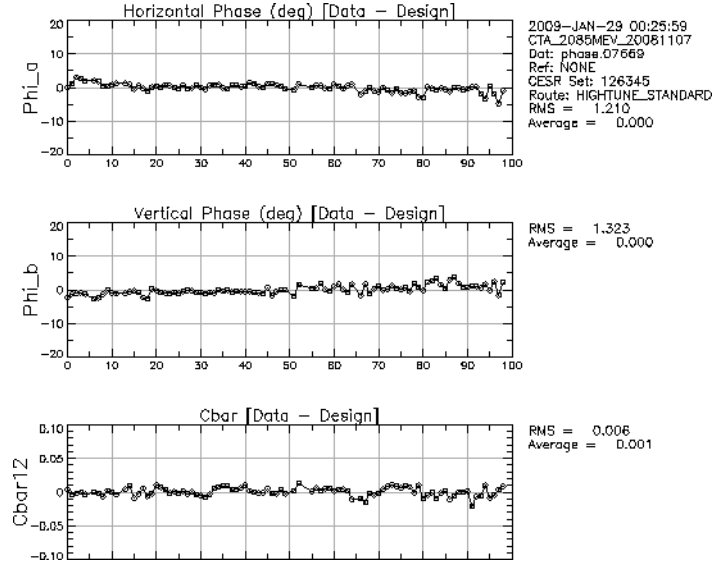


**Figure 7.** After applying phase and coupling correction to the data in the preceding figure. The two upper plots are the deviations from design for the betatron phases for the A-mode (horizontal-like) and B-mode (vertical-like) betatron dipole modes. The lower plot is the off-diagonal element of the  $\bar{C}$  horizontal-to-vertical coupling matrix. The horizontal scales on the plots are BPM number with the data set representing one complete cycle around CESR. The vertical scales for the phases are in degrees. The vertical scale for  $\bar{C}_{12}$  is unitless.

injector, triggered with each injection cycle, to measure the trajectory of the incoming bunches from the Synchrotron and 2) a single BPM in the Synchrotron, triggered at each injection cycle to quantify the amplitudes of oscillation for the bunches injected from the LINAC. At the time of this paper’s preparation, programming is underway for the Synchrotron BPM readout module.

The transfer line BPM readouts have been in routine use during 2016 and their performance has been under study. Injection from the LINAC and Synchrotron into CESR is a top-off process, where the charge per bunch may be 2 to 3 orders of magnitude lower than the stored beam current. As a result this requires the use the CBPM’s high gain amplifiers before digitization. The observations to date are summarized here qualitatively. After the modules’ amplifier gains are adjusted, the signals from the electron beam are typically large enough to have similar digitizer uncertainties as the stored beam. Even after applying full module gain amplification, the positron bunch signals are usually well less than the full scale for the digitizers, implying the digitizing error have a larger influence on the beam position measurements for the positron beam. When compared to the stored beam, the timing jitter from pulse-to-pulse is not expected to be a major problem, since the energy acceptance of the Synchrotron limits the acceptable timing jitter of LINAC to be  $\pm 5$  psec at an absolute maximum with the variation of timing for the beam extracted after acceleration in the Synchrotron is expected to be less than this.

The standard time in procedure many injection cycles to generate a timing scan (Figure 4) Due to pulse-to-pulse intensity variations of the Synchrotron beam, it is difficult to achieve as precise timing for each button as for CESR, using the standard timing algorithm. The measured variation of the electron beam position has uncertainties of  $\pm 0.32$  mm and  $\pm 0.34$  mm in the horizontal

and vertical direction, respectively. Most of the position uncertainties during operations are due to pulse-to-pulse positioning errors when the LINAC bunches are injected into the Synchrotron, which result in pulse-to-pulse variations in the position of Synchrotron bunches during extraction for injection into CESR.

### 3 Summary

This paper has described the upgrade of the CESR beam position monitoring instrumentation, which has been developed for use in the CESRTA program for the investigation of storage ring beam dynamics. In particular the new CBPM modules have achieved the design goals set for the CESRTA program. This has been an important tool for the CESRTA studies focusing on the methods for low emittance tuning of the beam[20], on the causes of intra-beam scattering of single bunches[21] and on the production and interaction of bunches within trains with electron clouds, which have been produced by photo-electrons from synchrotron radiation and secondary emission.

### References

- [1] M. Billing, *The conversion of CESR to operate as the Test Accelerator, CesrTA. Part 1: overview*, *J. Instrum.* **10** (July, 2015) .
- [2] M. G. Billing and Y. Li, *The conversion of CESR to operate as the test accelerator, CesrTA, part 2: Vacuum modifications*, *J. Instrum.* **10** (July, 2015) .
- [3] M. G. Billing, J. V. Conway, J. A. Crittenden, S. Greenwald, Y. Li, R. E. Meller et al., *The conversion of CESR to operate as the test accelerator, CesrTA, part 3: Electron cloud diagnostics*, *J. Instrum.* **11** (Apr., 2016) .
- [4] R. W. Helms and G. H. Hoffstaetter, *Orbit and optics improvement by evaluating the nonlinear beam position monitor response in the Cornell Electron Storage Ring*, *Phys. Rev. ST Accel. Beams* **8** (June, 2005) .
- [5] D. L. Rubin, M. Billing, R. Meller, M. Palmer, M. Rendina, N. Rider et al., *Beam based measurement of beam position monitor electrode gains*, *Phys. Rev. ST Accel. Beams* **13** (Sept., 2010) .
- [6] A. Wolski, D. Rubin, D. Sagan and J. Shanks, *Low-emittance tuning of storage rings using normal mode beam position monitor calibration*, *Phys. Rev. ST Accel. Beams* **14** (July, 2011) .
- [7] M. Palmer, J. Dobbins, D. Hartill and C. Strohman, *An upgrade for the beam position monitoring system at the Cornell Electron Storage Ring*, in *Proceedings of the 2001 Particle Accelerator Conference, Chicago, IL* (P. Lucas and S. Webber, eds.), pp. 1360–1362, IEEE, 2001.
- [8] J. C. Smith, M. A. Palmer, D. L. Rubin and D. C. Sagan, *Diagnosis of optical errors with a precision BPM system at CESR*, in *Proceedings of the 2003 Particle Accelerator Conference, Portland, OR* (J. Chew, P. Lucas and S. Webber, eds.), pp. 2267–2269, IEEE, 2003.
- [9] M. A. Palmer, J. A. Dobbins, B. Y. Rock, C. R. Strohman and J. R. Moffitt, *System level implementation of beam position monitors with local data processing capability for the Cornell Electron Storage Ring*, in *Proceedings of the 2003 Particle Accelerator Conference, Portland, OR* (J. Chew, P. Lucas and S. Webber, eds.), pp. 2473–2475, IEEE, 2003.
- [10] M. G. Billing, J. A. Crittenden and M. A. Palmer, *Investigations of injection orbits at CESR based on turn-by-turn BPM measurements*, in *Proceedings of the 2005 Particle Accelerator Conference, Knoxville, TN* (C. Horak, ed.), pp. 1228–1230, IEEE, 2005.

- [11] M. A. Palmer, M. G. Billing, R. E. Meller, M. C. Rendina, N. T. Rider, D. L. Rubin et al., *CESR beam position monitor system upgrade for CesrTA and CHESS operations*, in *Proceedings of the 2010 International Particle Accelerator Conference, Kyoto, Japan*, pp. 1191–1193, ACFA, 2010.
- [12] A. Wolski, D. Rubin, D. Sagan and J. Shanks, *Normal mode BPM calibration for ultralow emittance tuning in lepton storage rings*, in *Proceedings of the 2011 International Particle Accelerator Conference, San Sebastián, Spain*, pp. 1114–1116, EPS-AG, 2011.
- [13] *The CESR Test Accelerator electron cloud research program: Phase I Report*, Tech. Rep. CLNS-12-2084, LEPP, Cornell University, Ithaca, NY, Jan., 2013.
- [14] R. Helmke, D. Rice and S. Ball, *Interface Hardware for the CESR Control System*, *IEEE Trans. Nuclear Science* **26** (June, 1979) .
- [15] M. J. Forster, S. Ball, L. Bartnik, D. Bougie, R. Helmke, M. Palmer et al., *CESR control system upgrade to linux high availability cluster*, in *Proceedings of the 2012 International Particle Accelerator Conference, New Orleans, LA*, pp. 3999–4001, IEEE, 2012.
- [16] C. Strohman and T. Wilksen, *CBI\_NET reference*, tech. rep., Cornell University, 2006.
- [17] M. Billing, *Introduction to beam diagnostics and instrumentation for circular accelerators*, in *Proceedings of the 1992 Beam Instrumentation Workshop*, pp. 55–77, 1992. DOI.
- [18] M. Billing, *Unpublished calculation*, tech. rep., Cornell University, 2012.
- [19] D. Sagan, R. Meller, R. Littauer and D. Rubin, *Betatron phase and coupling measurements at the Cornell Electron/positron Storage Ring*, *Phys. Rev. ST Accel. Beams* **3** (Sept., 2000) .
- [20] J. Shanks, D. L. Rubin and D. Sagan, *Low-emittance tuning at the Cornell Electron Storage Ring Test Accelerator*, *Phys. Rev. ST Accel. Beams* **17** (Apr., 2014) .
- [21] A. Chatterjee, K. Blaser, W. Hartung, D. Rubin and S. Wang, *Fast ion instability at the Cornell Electron Storage Ring Test Accelerator*, *Phys. Rev. ST Accel. Beams* **18** (June, 2015) .